The rapid transition from shallow to precipitating convection as a predator–prey process

Cristian V. Vraciu[1,2], Julien Savre[3], Maxime Colin[4]

[1]Faculty of Physics, University of Bucharest, Bucharest–Măgurele, Romania
[2]Department of Theoretical Physics, Horia Hulubei National Institute of Physics and Nuclear Engineering, Măgurele, Romania
[3]Meteorology Institute, Ludwig-Maximilians-Universität München, Munich, Germany
[4]Leibniz Centre for Tropical Marine Research, Bremen, Germany

Key Points:

- A conceptual picture for cumulus cloud populations based on cloud–updraft interaction is discussed
- The local shallow preconditioning and the cold pool feedback imply a predator–prey type of interaction in the cloud–precipitation system
- A simple predator–prey model shows good agreement with idealized numerical simulations for the rapid shallow–to–deep transition.

Corresponding author: Cristian V. Vraciu, `cristian.vraciu@theory.nipne.ro`

Abstract

Properly predicting the rapid transition from shallow to precipitating atmospheric convection within a diurnal cycle over land is of great importance for both weather prediction and climate projections. In this work, we consider that a cumulus cloud is formed due to the transport of water mass by multiple updrafts during its life–time. Cumulus clouds then locally create favorable conditions for the subsequent convective updrafts to reach higher altitudes, leading to deeper precipitating convection. This mechanism is amplified by the cold pools formed by the evaporation of precipitation in the sub-cloud layer. Based on this conceptual view of cloud–cloud interactions which goes beyond the one cloud equals one–plume picture, it is argued that precipitating clouds may act as predators that prey on the total cloud population, such that the rapid shallow–to–deep transition can be modeled as a simple predator–prey system. This conceptual model is validated by comparing solutions of the Lotka-Volterra system of equations to results obtained using a high-resolution large-eddy Simulation model. Moreover, we argue that the complete diurnal cycle of deep convection can be seen as a predator–prey system with varying food supply for the prey. Finally, we suggest that the present model can be applied to weather and climate models, which may lead to improved representations of the transition from shallow to precipitating continental convection.

Plain Language Summary

The rapid transition from shallow to precipitating convection over land is still poorly represented by weather and climate models. In this work, we argue that this is due to the fact that the convective parameterization schemes only consider the interaction between the clouds and their environment, which is a slow process, and do not consider cloud–cloud interactions during the transition, which is a fast process. We show that this latter interaction can be modeled as a predator–prey process, and we show how a very simple dynamical model for cloud population can lead to improved prediction for the precipitation rate and cloud cover over land.

1 Introduction

Atmospheric convection transports heat and moisture from the surface throughout the troposphere creating cumulus and cumulonimbus clouds that are responsible for the water cycle in the atmosphere and have a strong radiative forcing that can lead to either warming or cooling of the atmosphere. Shallow cumulus clouds are non–precipitating, or weekly precipitating convective clouds that form when the updraft plumes from the boundary layer reach the lifting condensation level but are unable to reach higher altitudes as they lose their buoyancy very quickly. Predicting shallow clouds is very important for climate predictability as they cover a very large part of the Earth and have a strong cooling effect on the climate system since they reflect an important fraction of the solar radiation back into space. When the atmosphere is unstable and the updraft plumes are able to reach the level of free convection, deep, precipitating convection is initiated. The deep convective clouds (congestus and cumulonimbus) precipitate, and re–stabilize the atmosphere as they warm and dry their environment. Since the cumulonimbus clouds are responsible for the formation of cirrus clouds, they also play a very important role in controlling the radiative budget of the Earth, as the cirrus clouds have a net warming effect. Therefore, the manner shallow and deep convective clouds are represented in climate models has a significant impact on climate predictions.

In general, the presence of a convective inhibition (CIN) layer prevents boundary layer updrafts from spontaneously reaching their level of free convection and slows down the development of deep precipitating clouds: in this situation, shallow cumuli develop first and contribute to the creation of conditions favorable to deep convection. The tran-

sition from shallow to precipitating convection can be considered of two types: (i) a slow transition when at the beginning the atmosphere is not unstable enough to sustain the development of precipitating convection, and the shallow cumuli slowly moisten the atmosphere until the environment is unstable enough to allow the clouds to grow deeper and precipitate (Yano & Plant, 2012b; Champouillon et al., 2023), which is a process that takes typically a few days; (ii) a rapid transition in which the atmosphere is already unstable but deep precipitating convection still takes a few hours to develop. This rapid transition occurs usually over the tropics where the atmosphere is always unstable (Hohenegger & Stevens, 2013). In a diurnal cycle over land, the rapid transition has been documented by several authors (Grabowski et al., 2006; Khairoutdinov & Randall, 2006; Kurowski et al., 2018; Grabowski, 2023; Savre & Craig, 2023). In this particular case, the transition starts when the convective inhibition becomes small, and it takes around 3-4 hours for precipitation to properly develop, despite having a very large convective available potential energy (CAPE) from the beginning. In this study, we focus on the second kind of shallow–to–deep transition.

Although in recent years many studies investigated the physical processes controlling the rapid transition from shallow to precipitating convection (Kurowski et al., 2018; Peters et al., 2022; Powell, 2022; Rochetin et al., 2014; Schiro & Neelin, 2019), weather and climate models still predict the onset of deep precipitating convection to occur around 2-5 hours earlier when compared to observations (Christopoulos & Schneider, 2021) or large–eddy simulation (LES) (Bechtold et al., 2004; Grabowski et al., 2006; Couvreux et al., 2015; Harvey et al., 2022; Tao et al., 2023) within a diurnal cycle over land. That is because the convective parameterization schemes immediately switch to deep convection when CIN is very small and CAPE is large, although in reality, even when these conditions are met, the transition still takes a few hours, or may not even occur within a diurnal cycle (Khairoutdinov & Randall, 2006; Nelson et al., 2021; Tian et al., 2021; Zhuang et al., 2017).

The majority of convective parameterization schemes used in climate models are based on the so–called mass–flux parameterization. The objective of these parameterizations is to find the mass flux of the clouds and to provide feedback to the large–scale resolved by the model. The mass–flux formulation is based on the idea that the clouds, or the whole ensemble of clouds, can be modeled as steady–state plumes. In the picture used by these formulations, a convective cloud is formed by only one entraining plume, which only entrains environmental air described by the mean resolved state (Arakawa, 2004; Plant, 2010; Yano, 2014). Thus, the mass flux is estimated in these parameterization schemes only by considering the large–scale state, neglecting any cloud–cloud interaction or heterogeneity within a given grid box. As the mass flux only changes with the slow change of the large–scale state, these schemes are unable to catch any rapid transition from shallow to precipitating convection (Bechtold et al., 2004). At the time Arakawa and Schubert (1974) formulated their parameterization, the grid box and the time–stepping used by climate models were so large that over the tropical ocean one could consider that at all times within a grid–box there is a spectrum of shallow and precipitating clouds that are in quasi–equilibrium with their environment. Many operational parameterization schemes still follow the original mass–flux formulation introduced by Arakawa and Schubert (1974) (e.g., Bechtold et al., 2014; Kain & Fritsch, 1993; Rio et al., 2019). However, nowadays, climate models have much finer resolutions, both in space and time, and the quasi–equilibrium is therefore not satisfied in every grid box at every time step (Davies et al., 2013; Donner & Phillips, 2003; Jones & Randall, 2011). To improve the representation of atmospheric convection in numerical models with high temporal resolution, several prognostic closures for the convective mass flux with relaxed quasi–equilibrium have later been formulated (e.g., Moorthi & Suarez, 1992; Pan & Randall, 1998; Wagner & Graf, 2010; Yano & Plant, 2012a)

In general, the time evolution of the convective mass flux at cloud base M_c can be written as:

$$\frac{dM_c}{dt} = \rho_0 \sigma_c \frac{dw_c}{dt} + \rho_0 w_c \frac{d\sigma_c}{dt}, \tag{1}$$

where t is the time, ρ_0 is the atmospheric density at the cloud base, σ_c is the convective cloud cover, and w_c is the convective updraft velocity of the convective clouds. The mass-flux parameterizations usually consider that σ_c is constant, and thus, only the first term on the right hand side (rhs) of Equation 1 is important. Although the traditional mass–flux formulations do not make the assumption that σ_c is constant in an explicit way, such an assumption can be easily justified if the grid box and the time step are very large, such that the fluctuations in σ_c are subgrid, and the increase in cloud population in a small subdomain is compensated by the decay of clouds in another small subdomain. Therefore, in the mass–flux parameterization schemes, the triggering of individual convective clouds is not considered, but rather the whole spectrum of clouds that slowly interacts with the large–scale environment (Yano et al., 2013). It should also be noted that parameterization models that implement a momentum equation for w_c have been formulated (e.g., Donner, 1993; Bechtold et al., 2001; Bretherton et al., 2004), in which the assumption that σ_c is constant is made in an explicit way. As in the original mass–flux formulation based on quasi–equilibrium, the prognostic formulations of Pan and Randall (1998) and Wagner and Graf (2010) also consider a constant σ_c, and a steady–state plume that only interacts with a homogeneous environment. On the other hand, Yano and Plant (2012a, 2012b) assume that the time evolution of the mass flux is only controlled by the convective cloud cover, but it also considers the steady–state plume model while completely neglecting any cloud–cloud interaction.

Within a diurnal cycle over land, however, if the atmosphere is already unstable in the morning, the convection develops quite rapidly, while the cloud environment remains rather steady during the day (Tian et al., 2021). In such cases, one can no longer assume that the convection only interacts with the environment, and thus, convective memory might be important (Colin et al., 2019; Daleu et al., 2020; Colin & Sherwood, 2021; Hwong et al., 2023). Although the above mentioned prognostic formulations also introduce convective memory into their formulation, this is achieved based on *ad-hoc* relations, and not based on physical considerations. The main assumption in these prognostic formulations is that M_c does not respond immediately to changes in the large–scale state. However, it is not clear why such an assumption might be true for a steady–state plume that only interacts with a homogeneous environment. In the present work, we assume that the updraft velocity at cloud base only exhibits a slow change during the rapid shallow–to–deep transition over land (e.g., Figure 15 of Kurowski et al., 2018), whereas the cloud fraction of the precipitating clouds evolves from zero in the morning to a maximum around noon, and thus, for this particular case, the second term in the rhs of Equation 1 becomes significant. Thus, the scope of this study is to find a dynamical system able to represent the evolution of σ_c during the rapid transition from shallow to precipitating convection.

To predict the onset of deep precipitating convection, some numerical models assume CIN type triggering functions, which are used to turn on the deep convection scheme only if the updraft plumes in the boundary layer have a kinetic energy greater than CIN (Rio et al., 2009, 2013). However, such an implementation does not change the basis of the parameterization schemes but only decides when the scheme is active or not. If the scheme assumes a constant σ_c, then σ_c will jump from zero before triggering to a fixed value at triggering, remaining constant as long as the deep convective scheme is active. The problem with this kind of triggering function is that it does not allow for deep convection to properly develop from shallow convection, which results in predicting the onset of precipitating convection several hours sooner. To ameliorate this problem, several

parameterization schemes assume that within a diurnal cycle, at the triggering, even if CAPE is very large, deep cumulonimbus clouds only form if cold pools are also present (e.g., Hohenegger & Bretherton, 2011; Suselj et al., 2019). However, since CAPE is already large at the triggering time, the convective scheme immediately creates precipitation, being unable to capture the transition from the non–precipitating shallow cumuli to the precipitating congestus clouds. Thus, they are unable to fully correct the time of precipitation onset, but keep the precipitation rate small until the cumulonimbus clouds develop. In this work, we propose a conceptual model for cumulus clouds that allow for a gradual evolution of σ_c when the triggering conditions are met, governed by a predator–prey–type dynamical system.

2 Conceptual Model

In our model the clouds are formed due to the transport of water by the updrafts from the boundary layer. In contrast with the mass–flux formulation, we do not consider that every cloud, or every cloud ensemble, is described by only one steady–state plume, but we consider that a cloud can be formed by the contribution of multiple unsteady convective elements — such as thermals (e.g., Scorer & Ludlam, 1953; Sherwood et al., 2013; Hernandez-Deckers & Sherwood, 2016) or starting plumes (Pinsky et al., 2022) — as also suggested by several authors (e.g., Malkus & Scorer, 1955; Moser & Lasher-Trapp, 2017; Morrison et al., 2020; Vraciu et al., 2023). Indeed, the pulsating behavior of clouds has been documented by both observational studies (e.g., Harrington, 1958; Koenig, 1963; Raymond & Blyth, 1989; Damiani et al., 2006) and numerical simulations (e.g., Zhao & Austin, 2005; Heus et al., 2009; Sakradzija et al., 2015; Peters et al., 2019), which may indicate the presence of successive convective elements within the clouds. Each convective element transports a finite mass of water from the boundary layer to the cloud layer, and the cloud dimension is given by the total amount of water transported by the set of convective elements that reach the condensation level in that given place of the cloud during its life–time, minus the amount of cloud water that evaporates due to mixing with the environment (detrainment). The episodic mixing model of Emanuel (1991) is in fact based on a very similar conceptual picture (see also Emanuel, 1993). Emanuel (1991) makes very clear that in his parameterization scheme, the small convective elements within the clouds are responsible for the convective transport: "I am explicitly attempting to represent the collective effects of an ensemble of individual, $\mathcal{O}$(100 m)–scale drafts, not of ensembles of $\mathcal{O}$(1 km)–scale clouds. These drafts, rather than whole clouds, are regarded as the fundamental agents of convective transport." Thus, in this picture, a cloud can be seen as analogous to a wall of bricks, and a convective element as a new brick fixed on the wall by the builder — the clouds are seen as a collection of water elements brought by a number of convective elements during the cloud life–time, in which every water element represents a brick in our wall. This building process can be visualized for the development of a real cumulonimbus cloud at Kjoenbongarit (2013) or for a congestus cloud at Strong (2017).

We consider here two types of clouds: (i) nonprecipitating shallow cumuli, which are those clouds with a top close to the boundary layer depth, covering a fraction σ_s — this type of clouds remain shallow as they are unable to gain buoyancy, or lose their buoyancy very quickly; and (ii) convective precipitating clouds, which are clouds that are able to gain some buoyancy and have a top much deeper than the boundary layer depth, covering a fraction σ_c. Here, we consider that the convective precipitating clouds have a top above 4 km. Therefore, the total cloud cover is $\sigma = \sigma_s + \sigma_c$. We consider that the difference between the shallow and convective precipitating clouds is that the shallow clouds decay only due to mixing (detrainment) into the environment, whereas the convective precipitating clouds decay also by precipitation. Although the shallow cumuli can also lightly precipitate, we consider that the precipitation rate of shallow cumuli can be neglected with respect to the precipitation rate of convective precipitating clouds.

We consider that the total mass m_j of cloud j is given by:

$$m_j = \sum_{i}^{n} \delta m_i - m_{D,j}, \tag{2}$$

where δm_i is the mass transported into the cloud by the convective element i, n is the total number of convective elements that contribute to cloud j during its life–time, and $m_{D,j}$ is the mass lost by the cloud due to mixing with the dry environment and precipitation. Here, by cloud mass, we refer to the mass of air within a cloud, but other quantities might be considered as well, such as the mass of condensed particles (water plus ice), or the total integrated condensed water path. For the whole ensemble of clouds we can write:

$$m = \sum_{j} m_j = \overline{\rho}\sigma\overline{\Delta z}, \tag{3}$$

where m and $\overline{\Delta z}$ are the total mass and the average depth of the cloud ensemble, respectively, and $\overline{\rho}$ is the mean air density within the clouds. Here, all masses are per unit of area, so the masses in Equation 2 have units of kg m^{-2}. For the evolution of m, neglecting the time change of $\overline{\rho}$, we thus have:

$$\frac{dm}{dt} = \overline{\rho}\sigma\frac{d\overline{\Delta z}}{dt} + \overline{\rho}\,\overline{\Delta z}\frac{d\sigma}{dt} = M_0 - D, \tag{4}$$

where M_0 is the sum of the contributions from all convective elements to the total mass flux at the condensation level and $D = d(\sum_j m_{D,j})/dt$, is the rate at which the cloud ensemble loses mass due to evaporation and precipitation. Therefore, the evolution of the cloud fraction becomes:

$$\frac{d\sigma}{dt} = \frac{M_0 - D}{\overline{\rho}\overline{\Delta z}} - \sigma\frac{d(\ln\overline{\Delta z})}{dt}. \tag{5}$$

For a shallow case at equilibrium, $M_0 - D = 0$, meaning that the new mass brought into the cloud layer by the convective elements is compensated by the detrainment into the environment. However, during the shallow–to–deep transition, $\overline{\Delta z}$ increases rapidly, and the second term in the rhs of Equation 5 is positive and contributes to a reduction of the total cloud cover. It should be noted that, during the transition, $M_0 - D$ may not be constant as for a shallow case at equilibrium, but we assume that the contribution from this term remains generally small compared to the second term in the rhs of Equation 5. Besides, it is clear that since the first term on the rhs is inversely proportional to $\overline{\Delta z}$, the contribution from $M_0 - D$ to the evolution of σ will decrease as the cloud layer depth increases. Equation 5 thus indicates that the mass conservation implies a reduction in the total cloud fraction during the rapid shallow–to–deep transition.

2.1 Local Moisture Preconditioning

Because the moisture of the cloud environmental layer has been observed to be an important factor in the transition from shallow to precipitating convection, some studies argue that the rapid transition from shallow to precipitating convection can be explained by the moistening of the cloud environment by the shallow cumuli (Holloway & Neelin, 2009; Waite & Khouider, 2010), which is known as the moisture preconditioning mechanism. This idea can be perhaps better understood if we consider the following plume model (Morrison, 2017):

$$\frac{dB}{dz} = -N^2 - \varepsilon B - \varepsilon \frac{g L_v q_{sE}(1 - \mathcal{R}_E)}{c_p T_E \Gamma}, \tag{6}$$

where B is the plume buoyancy, z is the vertical coordinate, N^2 is the squared buoyancy frequency, ε is the entrainment rate, g is the gravitational acceleration, L_v is the latent heat of vaporization, q_{sE} is the saturation mixing ratio of the environment, $\mathcal{R}_E$ is the environmental relative humidity, T_E is the temperature of the environment, c_p is the specific heat of air at constant pressure, and $\Gamma \approx 1 + L_v^2 q_{sE}/(c_p R_v T_E^2)$ is a parameter, for which R_v is the water vapor gas constant. The last term in the rhs of Equation 6 represents the cooling rate of the updraft plume due to the evaporation of the cloud water that mixes with the dry environmental air. Thus, as shallow cumuli continue to increase RH_E, this term will continue to decrease, allowing the plumes to deepen the cloud layer (Morrison et al., 2022). However, Hohenegger and Stevens (2013) showed that the moisture preconditioning acts at time scales too long to explain the rapid transition. Note that the concept of preconditioning as formulated by Waite and Khouider (2010) or Yano and Plant (2012b) is based on the same consideration as the mass–flux formulation, with steady plumes that entrains air described by a mean domain value.

On the other hand, Vraciu et al. (2023) discussed the role of passive shallow cumuli in the transition from shallow to deep convection, which can be regarded as local moisture preconditioning. As in the moisture preconditioning mechanism described by (e.g., Waite & Khouider, 2010), the idea is that if the updraft plumes can entrain moister air, they will be able to grow deeper due to a smaller contribution of the last term in the rhs of Equation 6. However, the main difference is that we no longer assume a steady–state plume that entrains air only described by a mean state, as in the mass–flux formulation, but we consider that the plumes (or any other convective elements) have a smaller life–time than the clouds, and are allowed to develop in the place of existing clouds. Thus, the cloud itself provides a local preconditioning for the development of the subsequent convective elements, as also shown by Moser and Lasher-Trapp (2017). This process of interaction between the convective elements and the existing clouds leads to deeper and deeper clouds. Furthermore, we can also consider that the clouds, even after a complete decay, still leave spots of abnormally large humidity that slowly dissipate into the environment (e.g. Figure 7 of Daleu et al., 2020). Thus, if the convective elements reach the condensation level in the location of such spots, they will again benefit from the local preconditioning, creating deeper clouds. We may also consider that the area of these spots is proportional to the total cloud cover at the cloud base.

Let us consider that at a given time we have a cloud field of shallow cumuli, as schematically presented in Figure 1A. We consider that every cloud, either shallow or deep, is formed by a set of convective elements that transported water from the boundary layer to the cloud layer. After a given time, a new set of convective elements reaches the condensation level. Here, we have two possibilities: (i) the convective elements reach the condensation level in a place where there are no clouds (or spots of large humidity), forming new shallow cumuli. This case is schematically illustrated in Figure 1B. At the same time, some of the clouds decay during the development of the new convective elements, and thus, we can consider that the new clouds statistically replace the old ones that died; (ii) the new set of convective elements reach the condensation level in the place of an already existing cloud, as schematically illustrated in Figure 1C. In this case, the convective elements will transport water from the boundary layer in a higher cloud layer, while some of the shallow clouds decay. As a result, the total cloud fraction σ decreases, while the fraction of clouds that become convective σ_c increases.

As convection becomes more intense, the compensating entrainment of dry air from the cloud layer into the boundary layer also increases, which creates a stable transition layer between the top of the boundary layer z_i and the lifting condensation level (LCL) (Betts, 1976; Neggers et al., 2006; Albright et al., 2022). As a result, the mass flux of

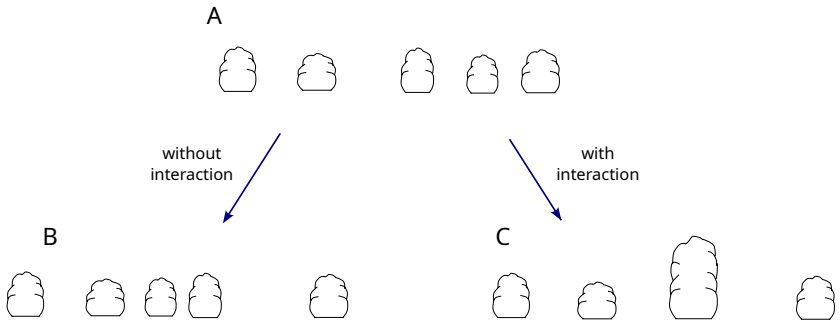

Figure 1. Deepening of a cumulus clouds due to local preconditioning. (A) initial cloud field with five shallow cumuli. (B) after a time, one of the clouds decays, while a new set of convective elements, that do not interact with the existing clouds, forms a new shallow cumulus. As a result, the cloud fraction remains steady. (C) as in (B), but now the new set of convective elements develop in the place of one of the existing clouds, forming a deeper, convective precipitating cloud. As a result, the cloud fraction at cloud base decreases, while the cloud fraction of convective precipitating cumuli increases.

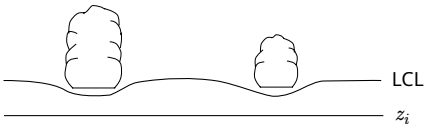

Figure 2. Schematics of non–precipitating clouds altering the transition layer between z_i and LCL.

the updrafts at cloud base may also decrease as the number of convective precipitating clouds increases. Because the non–precipitating clouds always mix with the environment due to diffusion and turbulent mixing, we expect the air just below the base of a given non–precipitating cloud to be moister than the air at the same height but in a cloudless area (e.g. Albright et al., 2023). Thus, as the convective elements that develop in the place of an already existing cloud mix moister air than those developing in the cloudless areas, we consider that the non–precipitating clouds also create heterogeneity in the stable transition layer (Figure 2), making easier for the convective elements to reach the condensation level where there are already non–precipitating clouds present. This alteration of the transition layer is also supported by the findings of Vraciu et al. (2023) who showed that the fraction of convective elements that develop where a cloud is already present is comparable with the fraction of convective elements that develop in cloudless areas, even though the clouds only occupy a very small fractional area. Therefore, we expect the fraction of updrafts at the cloud base to also decrease with the decrease of σ, which leads to a further reduction in σ. The local shallow preconditioning thus leads to deeper clouds, which due to mass conservation and alteration of the transition layer leads to a reduction in the cloud cover at cloud base.

2.2 Cold Pools Feedback

Once the clouds begin to precipitate, cold pools are formed in the boundary layer, which organize the convective field. This organization can be seen as updrafts being larger and more organized (Schlemmer & Hohenegger, 2014; Meyer & Haerter, 2020). This leads to further deepening of the cloud layer for two reasons: firstly, the larger convective el-

ements experience smaller entrainment (Kurowski et al., 2018; Schlemmer & Hohenegger, 2014), and thus, are able to better preserve their buoyancy, and secondly, more organized convective elements facilitate the local preconditioning, as the probability for a set of convective elements to develop in a certain place (to cluster) is larger. Although one may argue that the cold pools lead to convective elements that are so large that they do not require local preconditioning, Savre and Craig (2023) show that, during the transition, the increase in the updraft dimension is negligible compared with the increase in cloud dimension — there are no updrafts as large as a deep convective cloud, and thus, we argue here that cold pools essentially make the local preconditioning more efficient without substantially altering the properties of the boundary layer updrafts. In other words, we still consider that a convective cloud is a result of multiple convective elements bringing water from the boundary layer in the same location, but since the convective elements are larger and better organized, a smaller number of convective elements are required to build a precipitating cloud. Following the analogy between clouds and brick walls, we can picture the cold pool feedback as having sets of bricks that are already tied together, and thus, the building process is much more efficient since the builder brings a new set of tied bricks with only one move. Although we do not consider that it is impossible for only one convective element to create a precipitating cloud, we consider that even in this case, the convective element will benefit from the large humidity spots created by the non–precipitating clouds, and such a situation might rather correspond to the creation of "turkey towers" (e.g. Figure 7.14 in Markowski & Richardson, 2011), rather than the creation of congestus or cumulonimbus clouds.

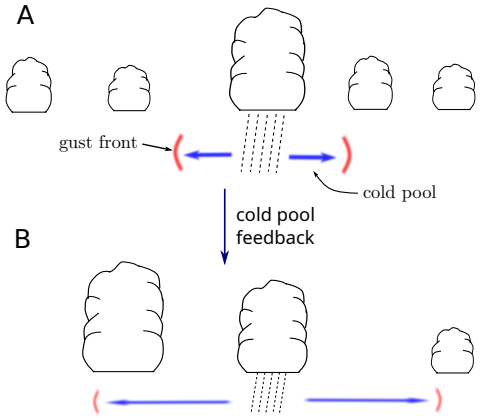

Figure 3. Deepening of a cumulus clouds due to cold pool feedback. (A) initial cloud field with four shallow clouds and one convective cloud in the decaying precipitating stage, which creates a cold pool that leads to the development of a new convective precipitating cloud at a later time (B). At the same time, some of the shallow clouds decay without being replaced by new shallow cumuli. As the precipitating clouds, being deeper, occupy a smaller fraction than the shallow cumuli, for the same amount of building convective elements, the total cloud cover decreases.

In Figure 3, we illustrate the effect of the cold pools in the deepening of subsequent convection. Initially, we consider a field of shallow and precipitating clouds. The precipitating cloud illustrated in Figure 3A precipitates, creating a cold pool, and a new convective precipitating cloud is formed later on, as schematically illustrated in Figure 3B. Since the convective elements are larger and more organized, more water is transported by them to higher altitudes, which leads to a net decrease in the total cloud field. Moreover, although the cold pools trigger new updrafts at their gust fronts (Torri et al., 2015; Meyer & Haerter, 2020), as the cold pools represent areas of evaporatively cooled down-

drafts they also inhibit updrafts from developing within these areas. The cold pools thus make the convective elements to be fewer but stronger (e.g. Figure 15 of Kurowski et al., 2018). Therefore, we also expect a reduction in the updraft fraction at the cloud base due to cold pool feedback.

2.3 Predator-Prey Model

The physical processes discussed above suggest that the transition from shallow to precipitating convection can be modeled as a predator-prey process with convective precipitating clouds acting as predators, and the total cloud field acting as prey. We consider that the prey is represented by the total cloud field as both the shallow and convective precipitating clouds precondition their local environment, as long as the convective precipitating clouds are not in the decaying precipitating stage. However, we consider that the fraction of clouds in the decaying precipitating stage is much smaller than the total cloud fraction.

Here, for simplicity, we consider a very simple predator–prey model, namely the Lotka–Volterra model (Takeuchi, 1996), given by:

$$\frac{dx}{dt} = ax - bxy, \tag{7}$$

$$\frac{dy}{dt} = exy - fy, \tag{8}$$

where x is the population of prey and y is the population of predators, and a, b, e, and f are system coefficients. A solution of the Lotka–Volterra system is presented in Figure 4.

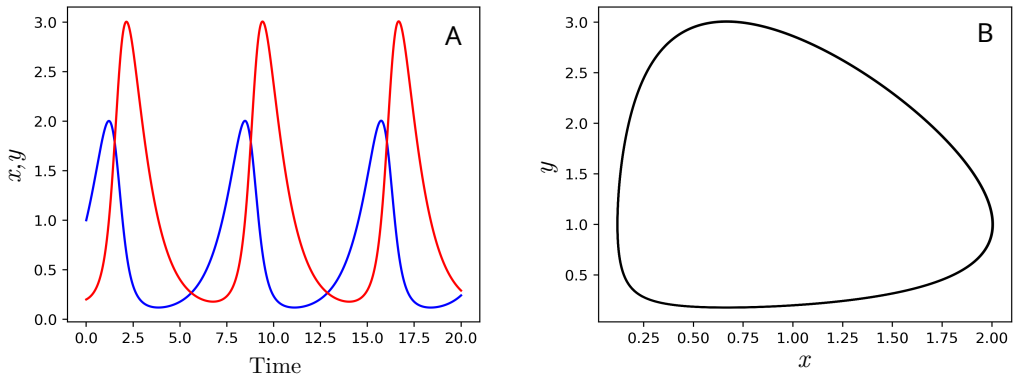

Figure 4. Solution of the Lotka–Volterra system. (A) Time evolution of prey (blue solid line) and predators (red solid line); (B) Limit cycle of the system.

In our case, we consider that the prey is played by the total cloud population at cloud base, which sustains the development of the deeper clouds, that act as predators. Thus, we consider $x = \sigma$ and $y = \sigma_c$. The first term in the rhs of Equation 7 represents the difference between the source of new convective elements from the boundary layer and the decay of the old clouds due to the mixing with the environment and precipitation. In the absence of precipitation, all the clouds are shallow. As shallow cumuli moisten their environment, we expect the shallow cloud cover to increase as the life–time

of the clouds increases due to mixing with moister and moister air. Thus, in the absence of precipitation, the shallow cloud cover grows exponentially, which might correspond to a cumulus–to–stratiform transition, rather than the case considered here. The second term represents the decay in the cloud cover due to interactions between precipitating clouds and the rest of the cloud population. σ_c appears in this term for two reasons: firstly, the deeper clouds have longer life–times and are wider, hence increasing the probability for new convective elements to interact with them, and secondly, when they precipitate, they form cold pools that trigger new precipitating clouds thus further decreasing the total cloud cover (see Section 2.2). The first term on the rhs of Equation 8 represents the growth of convective precipitating clouds for the same physical arguments as for the second rhs term of the prey equation. Lastly, the last term in the rhs of Equation 8 represents the decay rate of convective precipitating clouds due to precipitation and dissipation into the environment. An important limitation of the Lotka–Volterra model, however, is that predators cannot be created from nothing, and thus, σ_c must be initialized with a nonzero value. Note that the predator–prey system described here comprises cannibalism as the total cloud population, including precipitating clouds, acts as a prey for the precipitating cloud population.

Although more realistic and accurate predator–prey models may be considered here, the Lotka–Volterra model was selected for its simplicity. Besides, it should be kept in mind that the coefficients of the predator–prey system may not be universal, but may rather depend on other meteorological parameters, such as environmental relative humidity, or the boundary layer depth, which are well–known to be important parameters in the shallow–to–deep transition (e.g., Morrison et al., 2022; Grabowski, 2023).

Similar predator–prey models for the cloud–precipitation system have previously been formulated by Colin and Sherwood (2021) and Koren and Feingold (2011), but based on completely different physical arguments, and not for the specific transition case discussed here. Our model also differs from the predator–prey model of Wagner and Graf (2010) where a Lotka–Volterra model was used to model interactions between cloud species, excluding cannibalism.

3 Tests and Extensions of the Predator-Prey Model

3.1 LBA Transition Case

Results obtained from a high-resolution large–eddy simulation (LES) were analysed in order to test our hypotheses. The model configuration constitutes an idealization of the original Large–scale Biosphere–Atmosphere (LBA) case described in Grabowski et al. (2006) with initial conditions and forcings taken from Böing et al. (2012). The relative humidity was held constant and equal to 80% up to an altitude of $6,000$ m, and then decreased linearly to 15% at $17,500$ m. The potential temperature was computed from a prescribed lapse rate following a simple function of altitude, while horizontal winds were initially set to 0 m s^{-1} everywhere. Latent and sensible surface heat fluxes were held constant throughout the simulation and equal to 343 W m^{-2} and 161 W m^{-2} respectively, which corresponds to the diurnal averages of the time-dependent fluxes imposed in Grabowski et al. (2006). Horizontal winds were nudged back to their initial values with a time scale of 6 hr over the course of the simulation, but no other external forcing (including radiation and large-scale advection) was imposed.

The simulation was performed using the MISU-MIT Cloud and Aerosol model (MIMICA; Savre et al., 2014) as described in Savre and Craig (2023). The numerical domain extends over 102.4 km in both horizontal directions, and the upper boundary is situated $14,250$ m above the surface. The horizontal grid spacing is equal to 100 m in both directions, while the vertical grid spacing is constant and equal to 25 m below 1500 m, but increases geometrically above to reach ~ 400 m in the topmost grid layer. Lateral bound-

aries are periodic, whereas the surface is considered as a free-slip boundary (no momentum fluxes).

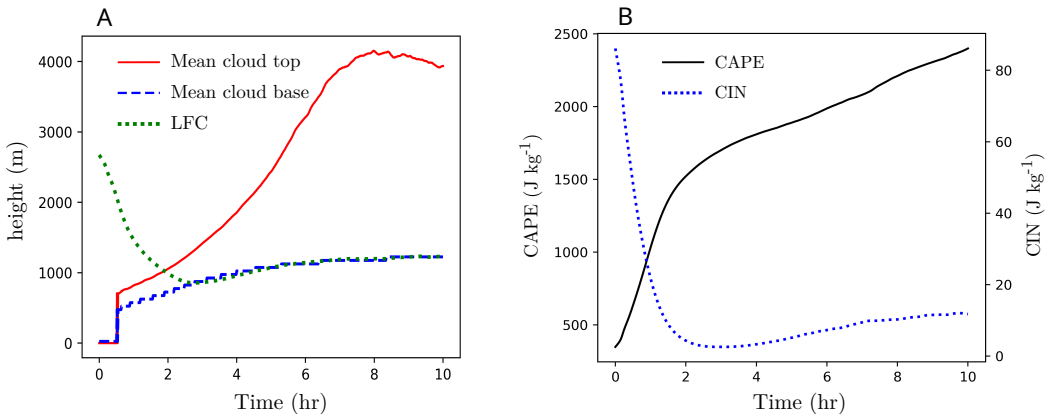

Figure 5. Shallow–to–deep transition in the idealized LBA case. (A) Time series of mean cloud top (red solid line), mean cloud base (blue dashed line), and LFC (green dotted line). (B) Time series of CAPE (black solid line) and CIN (blue dotted line).

The simulation was continued over a period of 10 hr, during which time-dependent variables were extracted every minute. The first clouds are observed 1 hr after the start of the simulation, whereas the onset of surface precipitation occurs 1.5 hr later. Overall, the transition from shallow-to-deep convection happens progressively over the first 7 hr of simulation. In Figure 5A, the mean cloud base and mean cloud top altitudes are shown. Here, the mean cloud base is defined as the level at which the cloud cover is maximum, and the mean cloud top is defined as the first vertical layer from the top where the condensed water mixing ratio exceeds 10^{-3} g kg^{-1}. Clouds are identified at locations where the condensed water mixing ratio exceeds a threshold of 10^{-3} g kg^{-1}. In addition, the level of free convection (LFC) is also represented. As one may see, after around 3 hr the mean cloud base altitude is almost identical to the LFC. The time evolution of CAPE and CIN is also represented in Figure 5B. CIN becomes very small after 2 hr, gradually increasing during the shallow–to–deep transition to about 10 J kg^{-1}. Here, we consider the shallow–to–deep convection transition to begin 2.5 hr after the start of the simulation. During the transition, CAPE increases from about 1600 J kg^{-1} to about 2000 J kg^{-1}.

The total cloud cover σ and cloud cover associated with precipitating convection σ_c that will be used to validate the predator–prey model are defined as follows. The total cloud cover is computed as the ratio between the number of grid cells identified as cloudy at the mean cloud base altitude to the total number of grid cells at that level. The cloud cover of convective precipitating clouds is defined following the same procedure but 4 km above the surface. In Figure 6A, simulated total and precipitating cloud covers are shown together with a solution of the Lotka–Volterra model in which the cloud fraction at cloud base (total cloud population) is assumed to act as prey, and the cloud fraction at 4 km (precipitating cloud population) is assumed to act as predator. The Lotka–Volterra model is solved using the simple Euler method with 10^4 iterations (a convergence test with 10^3 iterations has been performed, showing no significant difference). Here, the Lotka–Volterra model is represented only to show the predator–prey characteristic of the system, and thus, no objective tuning of coefficients against the LES data has been performed: the coefficients were simply chosen to visually match the LES data. As can be seen from Figure 6A, even a very simple predator–prey system can model reasonably

well the rapid transition from shallow to deep continental convection, however, far from being a perfect model. As speculated above, σ_c can indeed act as a predator. We show in particular that the cloud cover decreases as the fraction of convective clouds at a higher level increases. Later, as the total cloud cover decreases, the number of clouds that provide local preconditioning for the subsequent convection also decreases, and thus, the population of predators (precipitating clouds) will decrease as they no longer have enough preys to feed on.

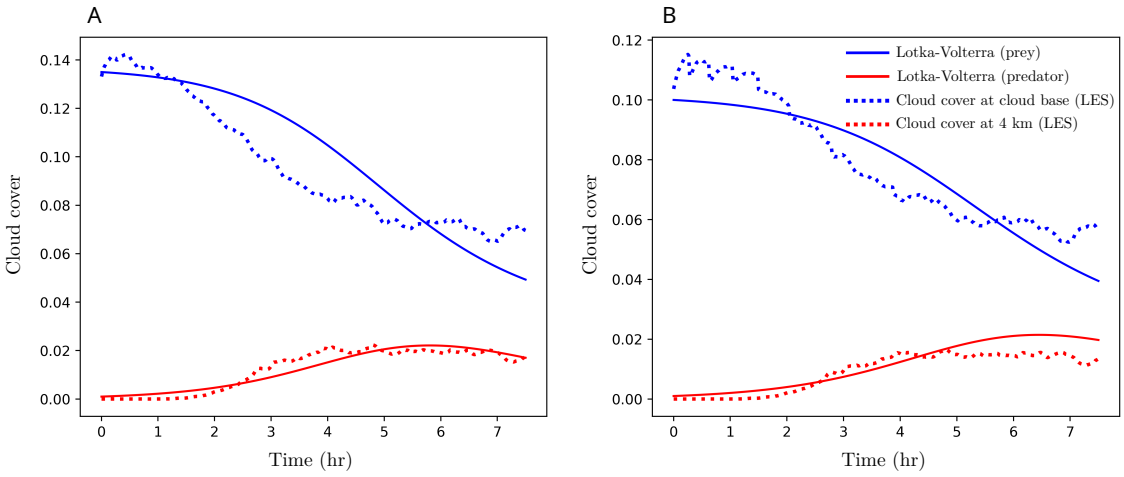

Figure 6. Lotka–Volterra model (solid lines) vs. LES data (dotted lines) for the LBA transition case. (A) Cloud cover at the cloud base as prey (blue lines) and cloud cover at 4 km height as predators (red lines). (B) As in (A) but for cloudy updraft cover. For the Lotka–Voltera model, the following coefficients are considered: $a = 0$, $b = 3 \cdot 10^{-3}$ s^{-1}, $e = 3.5 \cdot 10^{-3}$ s^{-1}, $f = 2.5 \cdot 10^{-4}$ s^{-1} (A); and $a = 0$, $b = 3 \cdot 10^{-3}$ s^{-1}, $e = 4 \cdot 10^{-3}$ s^{-1}, $f = 2 \cdot 10^{-4}$ s^{-1} (B). The initial conditions are set to 0.135 for the cloud cover at the cloud base, 0.1 for the cloudy updraft cover at the cloud base, and 10^{-3} for the cloud cover and for the cloudy updraft at 4 km. Here, the initial time is set to 2.5 hr after the start of the simulation.

Because the cloudy updrafts are regarded as the fundamental agents of vertical convective transport in the mass–flux parameterization, we also analyze here the predator–prey characteristics of cloud cover with clouds identified based on an additional updraft criterion. Here, a threshold of 0.1 m s^{-1} is used to identify the cloudy updrafts. The predator–prey characteristics of cloud cover based on this additional updraft criterion (cloudy updraft cover) are presented in Figure 6B. As speculated above, the cloudy updrafts cover also follows predator–prey characteristics, like the total cloud population. The predator–prey characteristics can be seen from the fact that the cloudy updraft cover at cloud base decreases as the cloudy updraft cover at 4 km increases in the first part of the transition. This is followed by a decrease in the cloudy updraft cover at 4 km as the number of prey becomes too small. Note that Yano and Plant (2012b) argue that during the shallow–to–deep transition, as CAPE increases, the cloudy updraft cover at cloud base also increases, but without giving any physical argument to support this assertion. However, it is quite clear from Figure 6B that for the rapid shallow–to–deep transition discussed here, the cloud cover at the cloud base exhibits a decrease during the transition, even though CAPE does increase.

As a first order approximation, we can consider that the surface precipitation rate P is directly proportional to σ_c. Similar to Koren and Feingold (2011), we may there-

fore replace σ_c with P in equations 7–8, thus considering that the surface precipitation rate acts as a predator that preys on the total cloud fraction. We then expect to see a time series for the cloud–precipitation system resembling that displayed on Figure 4A, and a solution for the cloud cover and precipitation rate similar to the one showed on Figure 4B.

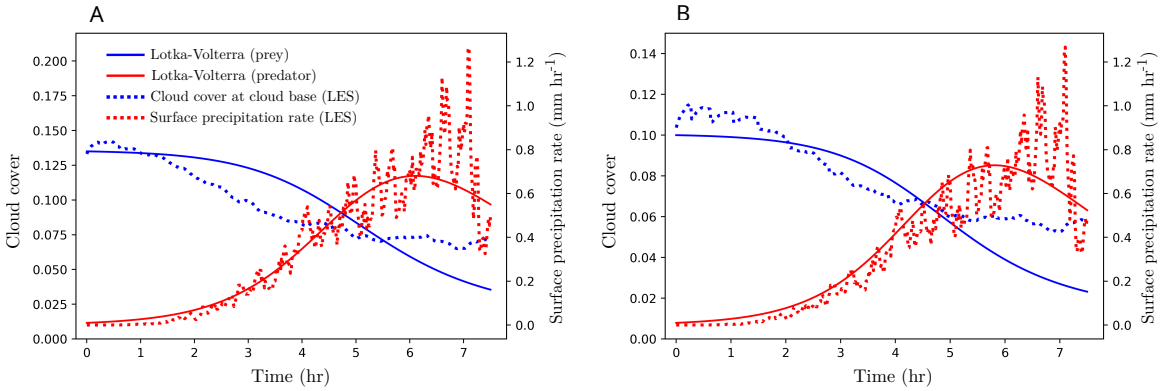

Figure 7. As in Figure 6 but the with surface precipitation rate acting as predators. For the Lotka–Voltera model, the following coefficients are considered: $a = 0$, $b = 1.5 \cdot 10^{-4}$ hr mm^{-1} s^{-1}, $e = 3.5 \cdot 10^{-3}$ s^{-1}, $f = 2 \cdot 10^{-4}$ s^{-1} (A); and $a = 0$, $b = 1.5 \cdot 10^{-4}$ hr mm^{-1} s^{-1}, $e = 5 \cdot 10^{-3}$ s^{-1}, $f = 2.1 \cdot 10^{-4}$ s^{-1} (B). The initial surface precipitation rate is set to 10^{-3} mm hr^{-1}.

In Figure 7, the time series of cloud cover at cloud base and surface precipitation rate are presented, together with a solution of the Lotka–Volterra model in which the cloud fraction at cloud base is assumed to act as prey, and the surface precipitation rate is assumed to act as predator. The surface precipitation rate displayed in Figure 7 represents the domain–averaged surface precipitation rate. Indeed, the cloud–precipitations system exhibits predator–prey characteristics during the rapid shallow–to–deep transition, as speculated above. Although not perfect, the Lotka–Volterra model does seem to represent reasonably well the interaction between clouds and precipitation.

3.2 Extension to a three species model

An extension to a three species model can be made by considering that the convective precipitating clouds can be further classified as congestus and cumulonimbus clouds. Here, we consider that the congestus clouds are those clouds with a top between 4 km and 8 km, whereas the cumulonimbus clouds have a top above 8 km. Therefore, we consider that the cloud cover at the cloud base (total cloud population) acts as prey for the cloud cover at 4 km σ_c (convective precipitating cloud population), which also represents the prey for the cloud cover at 8 km σ_{cb} (cumulonimbus cloud cover). Hence, we have the following predator–prey system:

$$\frac{d\sigma}{dt} = \beta_1\sigma - \beta_2\sigma\sigma_c, \tag{9}$$

$$\frac{d\sigma_c}{dt} = \beta_3\sigma\sigma_c - \beta_4\sigma_c\sigma_{cb} - \beta_5\sigma_c, \tag{10}$$

$$\frac{d\sigma_{cb}}{dt} = \beta_6\sigma_c\sigma_{cb} - \beta_7\sigma_{cb}, \tag{11}$$

where β_1–β_7 are system coefficients. A solution to this system is presented in Figure 8, together with time series of cloud cover at the cloud base (Figure 8A), 4 km (Figure 8B), and 8 km (Figure 8C), from the LBA transition case described above. Comparing the LES data for the cloud cover at these three levels with the solution of the Lotka–Volterra model, the system seems to exhibit predator–prey characteristics with three species.

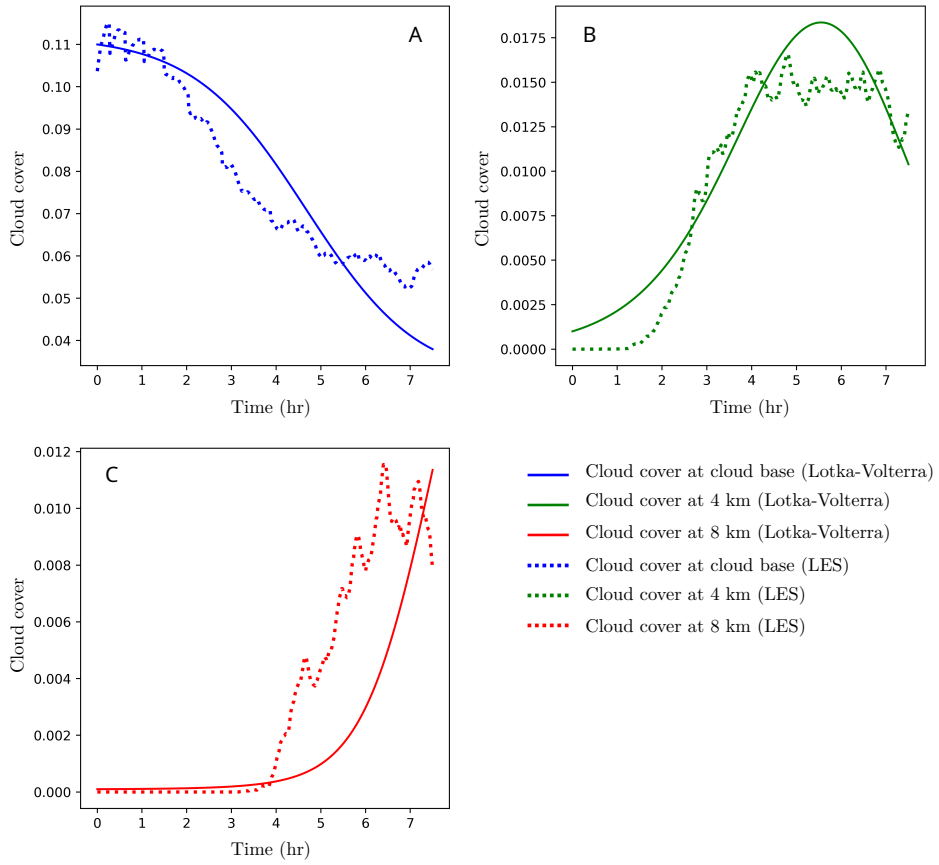

Figure 8. Three species Lotka–Volterra model (solid lines) vs. LES data (dotted lines) for the LBA transition case. (A) Cloudy updraft cover at the cloud base as prey (blue lines); (B) Cloudy cover at the 4 km height representing the convective fractional area of congestus and cumulonimbus clouds; (C) Cloudy cover at the 8 km height representing the convective fractional area of cumulonimbus clouds. For the Lotka–Voltera model, the following coefficients are considered: $\beta_1 = 0$, $\beta_2 = 3.8 \cdot 10^{-3}$ s^{-1}, $\beta_3 = 3.8 \cdot 10^{-3}$ s^{-1}, $\beta_4 = 10^{-2}$ s^{-1}, $\beta_5 = 2 \cdot 10^{-4}$ s^{-1}, $\beta_6 = 1.7 \cdot 10^{-2}$ s^{-1}, $\beta_7 = 10^{-6}$ s^{-1}. The initial conditions are set to 0.11, 10^{-3}, and 10^{-4} for the cloudy updraft cover at the cloud base, at 4 km, and 8 km, respectively.

Further extension to n_z species, where n_z represents the number of vertical levels used by the parent numerical model, follows immediately. For the updraft fractional area σ_k at the vertical level k, we now have:

$$\frac{d\sigma_k}{dt} = a_{k,k-1}\sigma_k\sigma_{k-1} - a_{k,k+1}\sigma_k\sigma_{k+1} + r_k\sigma_k, \tag{12}$$

where $a_{k,k-1}$, $a_{k,k+1}$, and r_k are system coefficients. The number of species represents the number of vertical levels of the parent numerical model between LFC and the equilibrium level.

3.3 LBA Transition Case with Suppressed Cold Pools

As discussed in Section 2, in our conceptual model, the predator–prey characteristics for the shallow–to–deep transition is due to the local moisture preconditioning, with the cold pool feedback only acting as a reinforcement. Thus, we argue that predator–prey behavior is expected even in the absence of the cold pools. To test this aspect, an additional simulation with suppressed cold pools is performed. The strategy proposed by Böing et al. (2012) was adopted here whereby potential temperature and water vapor mixing ratio tendencies below cloud base are nudged to their horizontally averaged values with a time scale of 10 min.

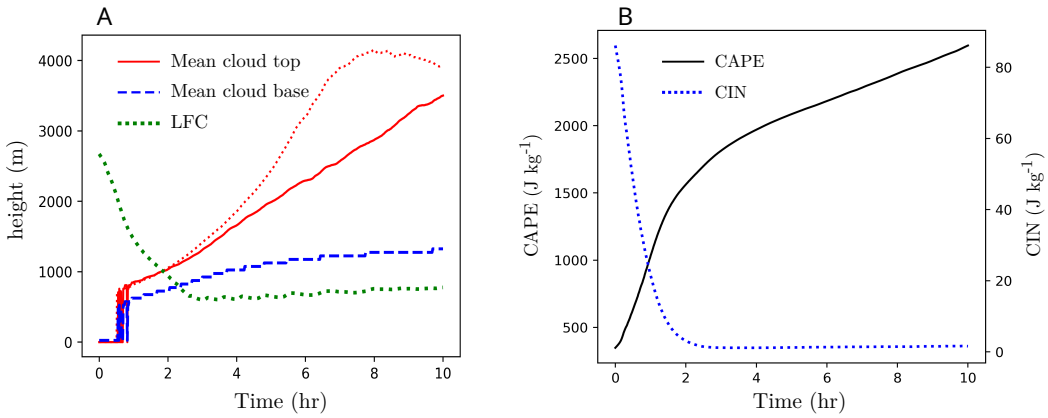

Figure 9. As in Figure 5, but for the case with suppressed cold pools. The mean cloud top for the case with active cold pools is also displayed here with red dotted line.

In Figure 9A, the mean cloud top, mean cloud base, and LFC are presented. The mean cloud top for the case with active cold pools is also presented here to better appreciate the cold pool feedback in the shallow–to–deep transition. As expected, the transition is slower for the case with suppressed cold pools, although there is not a large difference between the mean cloud top for the two cases in the first part of the transition, during which we argue that the role of local preconditioning is the main mechanism responsible for the transition. As another interesting aspect, in this case, the LFC is lower than the mean cloud base during the shallow–to–deep transition. As in the case with active cold pools, we consider that the transition starts at 2.5 hr after the start of the simulation, but the cloud top does not reach a maximum even after 10 hr, at the end of the simulation. The time series for CAPE and CIN is represented in Figure 9B. Although CAPE increases in a similar fashion to the case with active cold pools, CIN reaches a minimum after around 2.5 hr, remaining rather constant during the transition, at a value of about 1.5 J kg^{-1}. In addition, LFC is also much lower in the case with suppressed cold pools (around 0.7 km) than in the case with active cold pools (around 1 km).

In Figure 10, the cloudy updraft covers at cloud base, 4 km, and 8 km, are represented for the case with suppressed cold pools, together with a solution of the three species Lotka–Voltera model. As speculated, even without cold pools, the system seems to exhibit predator–prey characteristics. In order to appreciate the role of the cold pool feedback in the transition, we also represent the cloudy updrafts covers for the case with ac-

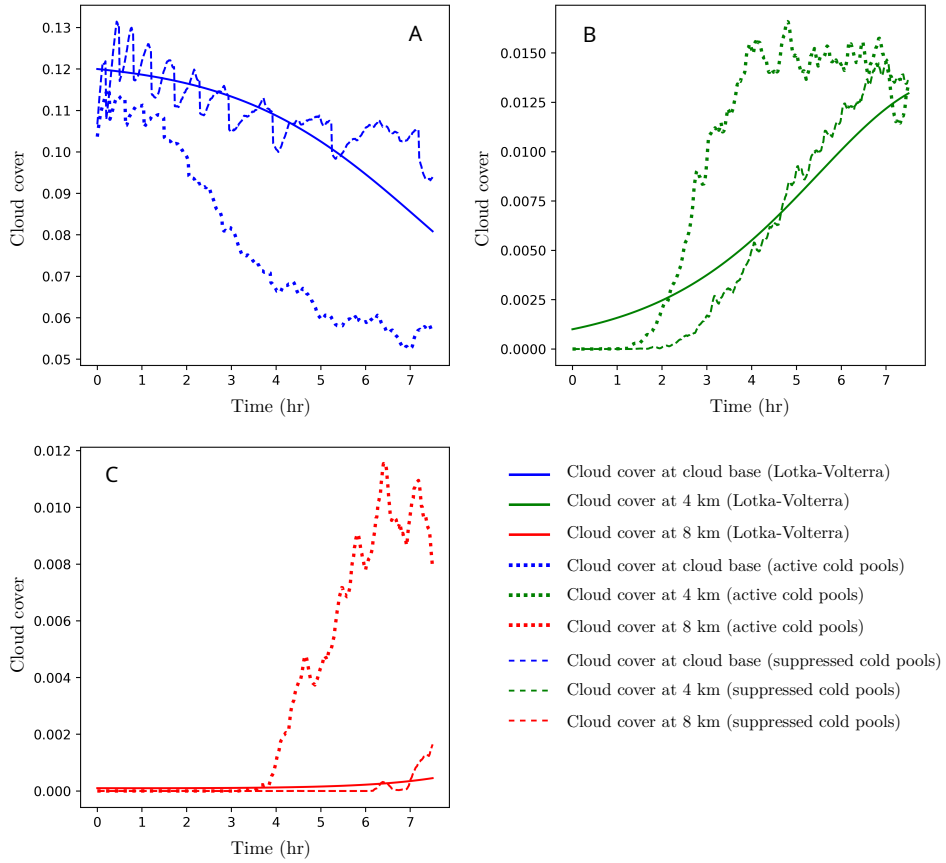

Figure 10. As in Figure 8, but for the case with suppressed cold pools. The cloudy updraft covers for the case with active cold pools are also displayed here with dotted lines, while the cloudy updraft covers for the case with suppressed cold pools are represented with dashed lines. For the Lotka–Voltera model, the following coefficients are considered: $\beta_1 = 0$, $\beta_2 = 2.5 \cdot 10^{-3}$ s^{-1}, $\beta_3 = 2.5 \cdot 10^{-3}$ s^{-1}, $\beta_4 = 10^{-2}$ s^{-1}, $\beta_5 = 1.7 \cdot 10^{-4}$ s^{-1}, $\beta_6 = 1.3 \cdot 10^{-2}$ s^{-1}, $\beta_7 = 2 \cdot 10^{-5}$ s^{-1}. The initial conditions are set to 0.12, 10^{-3}, and 10^{-4} for the cloudy updraft cover at the cloud base, at 4 km, and 8 km, respectively.

tive cold pools. As we expected from the conceptual model, without cold pool feedback the predators are not that efficient in preying on the total cloud population, and thus the cloud cover at the cloud base does not decrease as fast as the cloud cover for the case with active cold pools, while the populations of convective precipitating clouds and cumulonimbus clouds are not able to grow as fast and as much as for the case with active cold pools. Moreover, with suppressed cold pools, a larger number of updrafts are able to reach the condensation level as CIN is lower and there is no organization of the updraft field in the boundary layer.

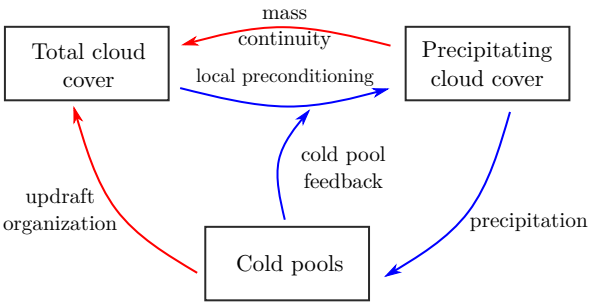

Figure 11. Schematics of feedback between the clouds and cold pools. The blue arrow denotes a positive causality, while the red one denotes a negative causality.

Although there is a significant difference in the number of cumulonimbus clouds between the two simulations, it is clear that the deepening of cumulus convection is possible even without cold pools feedback. This aspect, together with the predator–prey characteristics of the case with suppressed cold pools, indicates that the local preconditioning plays a major role in the shallow–to–deep transition, as also argued by Vraciu et al. (2023), and we believe that much more attention should be given to the local moisture preconditioning, and to the interplay between the local preconditioning and cold pools feedback during the transition from shallow to precipitating convection. We schematically present the feedback loops between the clouds and cold pools in our conceptual model on Figure 11. A negative feedback loop between the total cloud cover and precipitating cloud cover is possible without the presence of the cold pools, due to local preconditioning and mass continuity, implying a predator–prey–type of interaction between the two. As the precipitating clouds start to precipitate in their decaying state, cold pools are formed in the boundary layer, which have a positive effect on the population of precipitating clouds, but also a direct negative effect on the total cloud cover due to the organization of updrafts in the boundary layer, as discussed in Section 2.2. As the cold pools have a positive feedback on the population of precipitating clouds, due to mass continuity, the cold pools also have an indirect negative effect on the total cloud cover, as also schematically illustrated in Figure 3. Here, the arrow of the cold pools feedback points towards local preconditioning, as in our conceptual model the cold pools, through the organization of updrafts, increase the probability of updrafts feeding into preexisting clouds, and thus, leading to a larger degree of local preconditioning, as also discussed in Section 2.2. Overall, the cold pools amplify the feedback loop between the total cloud cover (prey) and the precipitating cloud cover (predator), which can be seen as making the predators more efficient in catching the prey. In this sense perhaps, the cold pools may be seen as mountains forcing the preys and predators to live into narrow valleys (the gust fronts), thus facilitating the interactions between them.

3.4 Complete Diurnal Cycle

To see if within a complete diurnal cycle the cloud–precipitation system exhibits predator–prey characteristics, we consider here the idealized case reported in Jensen et al. (2022) that is openly available at Haerter (2021). The reader is referred to Jensen et al. (2022) for case description and methodological details. In a complete diurnal cycle, we can no longer ignore the contribution of the surface heat flux on σ. Thus, we can no longer assume that the Lotka–Volterra system, in which there is no external forcing, can describe the interaction between the cloud cover and precipitation rate. However, during the transition from shallow to precipitation convection, we still expect to see a predator–prey type of interaction.

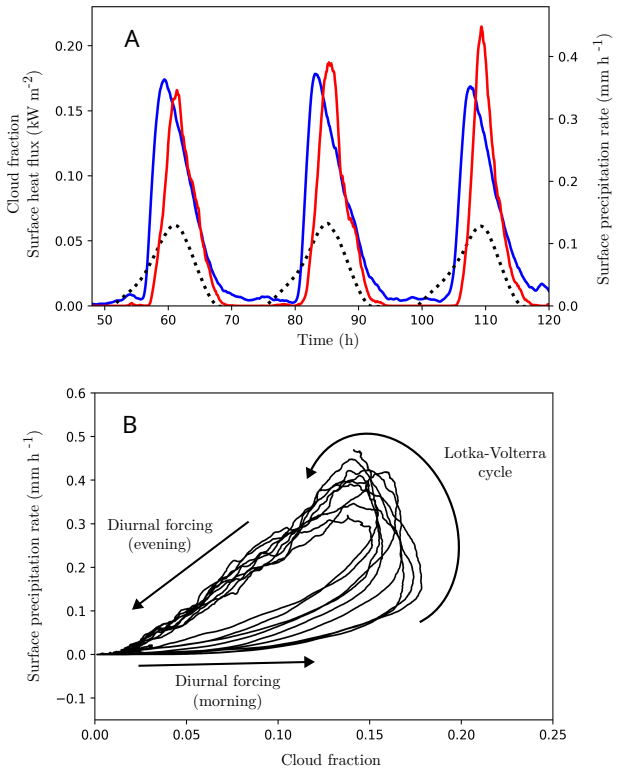

Figure 12. Large-eddy simulation of the cloud–precipitation system in a complete diurnal cycle from Jensen et al. (2022). (A) Time series for cloud fraction (blue solid line) and surface precipitation rate (red solid line) for three complete diurnal cycles. The surface heat flux is also represented for reference (dotted black line). (B) Limit–cycle of the cloud–precipitation system for the complete simulation (10 days), except the first two days, which are considered spin–up time.

In Figure 12, the LES data for cloud cover and surface precipitation from Jensen et al. (2022) are represented. In the morning, during the onset of the shallow convection, the cloud population increases as more and more updrafts are able to overcome the transition layer and reach the condensation level, and thus, the evolution of the cloud fraction is dominated by the diurnal forcing associated with the surface fluxes. As CIN approaches zero, the transition from shallow to precipitation convection starts, and indeed, during this short period, we see predator–prey characteristics in the cloud–precipitation system (Figure 12A), which correspond to the upper–right portion of the limit–cycle (Fig-

ure 12B). Thus, during the transition, in agreement with our conceptual model, the cloud fraction decreases as the precipitation rate increases, which in turn leads to a reduction in the precipitation rate. During the evening, as the surface heat flux is unable to provide enough energy into the system, and CIN is slowly restored. Thus, the cloud fraction decreases as the clouds that decay are no longer replaced by new active clouds, and the cloud population is again controlled by the diurnal forcing.

Although Figure 12 suggests that even within a complete diurnal cycle the system exhibits predator–prey characteristics, our simple Lotka–Volterra model is only able to represent the transition phase happening during the day. The model is indeed unable to represent the simultaneous decay of both shallow and deep cumuli at night when the reduced surface fluxes cannot sustain convection. A predator–prey model that takes into consideration this diurnal forcing might however be designed and adjusted to reproduce the complete diurnal cycle of cloud and precipitation. In this context, surface fluxes might be modeled as an external food supply for the preys in a biological system.

4 Discussion and Conclusions

In this study, we consider that the cumulus clouds are formed due to the upward transport of water vapor from the boundary layer by multiple convective elements, as suggested by empirical evidence. As the clouds themselves precondition their local surroundings for the subsequent convective updrafts, it is considered that the convective precipitating clouds act as predators, eating from the total cloud fraction that sustains their growth. As the clouds become deeper, the total cloud fraction decreases, and thus, the total cloud population can be seen as the prey population in a predator–prey system. It is also argued that the cold pool feedback acts as a reinforcement mechanism, leading to more clustered convection. The conceptual picture for the shallow-to-deep convection reminds us of the transition from unorganized to aggregated convection, but at a smaller scale. Therefore, we argue that the very complex cloud dynamics in the rapid shallow–to–deep transition of atmospheric convection can be described by the very simple Lotka–Volterra predator–prey system if it is assumed that the change in the large–scale state is slow enough during the transition. We tested a simple predator–prey model against idealized high–resolution LES data, showing good agreement between them. To isolate the role of local moisture preconditioning from that of cold pool feedback, we also consider a twin LES simulation with suppressed cold pools. In agreement with our conceptual model, the transition displays predator–prey characteristics even without cold pools, which might be an indication that the local preconditioning plays an important role in the shallow–to–deep transition. Finally, we discuss the complete diurnal cycle of deep convection, showing that the cloud population also exhibits a predator–prey–type of behavior in this situation. We consider that future research is required to study in depth every causality implied by our study, which might help us better understand the complex process of storm formation and convective organization.

In a diurnal cycle of deep continental convection, the predator–prey model assumes a gradual transition to deep convection instead of assuming an instantaneous deep convection triggering. The majority of current mass–flux schemes for deep convection consider a constant fractional area occupied by the convection, either explicitly or implicitly. However, in a rapid transition from shallow to precipitating deep convection, the environmental state only exhibits a small change, and the convective mass–flux is primarily controlled by convective fractional area and not by the vertical velocity. Therefore, our predator–prey model may be implemented for such a case by replacing the mass–flux predicted by the deep convection scheme M_c' with an adjusted mass–flux $M_{c,adj}$, as follows:

$$M_{c,adj} = \frac{\sigma_c}{\sigma_c'} M_c', \tag{13}$$

where σ_c is the fraction of convective precipitating clouds from the predator–prey model, and σ_c' is the constant fractional area assumed by the deep convection schemes. If the scheme does not assume a fractional area in an explicit way, then a constant value for σ_c' must be prescribed. Therefore, a predator–prey model may be implemented in a weather prediction or climate numerical model, obtaining a cumulus parameterization scheme with convective memory, that is based on a more realistic conceptual picture than the traditional mass–flux formulation, that goes beyond the one-cloud equals one-updraft framework. It should be noted, however, that this implementation cannot be made if the deep convective scheme already has a parameterization for the cold pool feedback (e.g., Rio et al., 2009; Suselj et al., 2019), as this would lead to a 'double counting' of the cold pools effect. Such an implementation, however, can only be made during the shallow–to–deep transition, as it is considered that the environment does not change substantially. Therefore, the predator–prey model must only be turned on when the conditions for deep convection onset are met and turned off after deep convection fully develops. Moreover, as shown in Section 3.2, the predator–prey system can be further generalized, to predict the convective fractional area at every vertical level of the numerical model. Future research is required to find the most appropriate predator–prey system for the shallow–to–deep transition and to tune the various coefficients introduced by the model.

As another very important contribution of the present conceptual model, a unified convection–cloud picture is described in which both clouds and convective elements interact with each other. Thus, the present predator–prey model also provides a parameterization for the total cumulus fraction, a problem notorious for the climate projections (e.g., Vogel et al., 2022). In addition, a complete unified parameterization might be built based on the principles introduced here by considering the prognostic Equation 5 for the cloud fraction, and a bulk plume model that considers the local preconditioning, as proposed for example by Vraciu et al. (2023). In the Vraciu et al. (2023) bulk plume model, a closure for the fraction of cloudy air entrained by the updrafts is required. However, based on the predator–prey model described here, it might be considered that the predators are those updrafts that only entrain moist cloudy air, obtaining thus the fraction as the ratio between the predators and the prey. Furthermore, note that by considering Equation 5, the boundary layer control of deep convection is implicit, in contrast with the traditional mass–flux formulation in which a boundary layer control, although considered by many modern parameterizations, might be in fact inconsistent with the steady–state plume model of the mass–flux formulation (please refer to Yano et al. (2013) for a detailed discussion of this issue). Such a development is not presented here but left for future work.

Open Research

The LES data presented in Sections 3.1 and 3.2 of this work are openly available at Savre (2023a), while the data presented in Section 3.3 are available at Savre (2023b). The data presented in Figure 12 are openly available at Haerter (2021).

Acknowledgments

The authors thank Robert Plant for insightful comments and feedback. CVV acknowledges financial support from the Romanian Ministry of Research, Innovation, and Digitization through Project PN 23 21 01 01 and from the Romanian Ministry of Education consisting in a doctoral scholarship received through the Doctoral School of Physics of the University of Bucharest.

References

Albright, A. L., Bony, S., Stevens, B., & Vogel, R. (2022). Observed subcloud-layer

moisture and heat budgets in the trades. *Journal of the Atmospheric Sciences*, *79*(9), 2363–2385.

Albright, A. L., Stevens, B., Bony, S., & Vogel, R. (2023). A new conceptual picture of the trade wind transition layer. *Journal of the Atmospheric Sciences*, *80*(6), 1547–1563.

Arakawa, A. (2004). The cumulus parameterization problem: Past, present, and future. *Journal of Climate*, *17*(13), 2493–2525.

Arakawa, A., & Schubert, W. H. (1974). Interaction of a cumulus cloud ensemble with the large-scale environment, Part I. *Journal of the Atmospheric Sciences*, *31*(3), 674–701.

Bechtold, P., Bazile, E., Guichard, F., Mascart, P., & Richard, E. (2001). A mass-flux convection scheme for regional and global models. *Quarterly Journal of the Royal Meteorological Society*, *127*(573), 869–886.

Bechtold, P., Chaboureau, J.-P., Beljaars, A., Betts, A., Köhler, M., Miller, M., & Redelsperger, J.-L. (2004). The simulation of the diurnal cycle of convective precipitation over land in a global model. *Quarterly Journal of the Royal Meteorological Society*, *130*(604), 3119–3137.

Bechtold, P., Semane, N., Lopez, P., Chaboureau, J.-P., Beljaars, A., & Bormann, N. (2014). Representing equilibrium and nonequilibrium convection in large-scale models. *Journal of the Atmospheric Sciences*, *71*(2), 734–753.

Betts, A. K. (1976). Modeling subcloud layer structure and interaction with a shallow cumulus layer. *Journal of the Atmospheric Sciences*, *33*(12), 2363–2382.

Böing, S. J., Jonker, H. J. J., Siebesma, A. P., & Grabowski, W. W. (2012). Influence of the subcloud layer on the development of a deep convective ensemble. *Journal of the Atmospheric Sciences*, *69*, 2682–2698. doi: 10.1175/JAS-D-11-0317.1

Bretherton, C. S., McCaa, J. R., & Grenier, H. (2004). A new parameterization for shallow cumulus convection and its application to marine subtropical cloud-topped boundary layers. Part I: Description and 1D results. *Monthly Weather Review*, *132*(4), 864–882.

Champouillon, A., Rio, C., & Couvreux, F. (2023). Simulating the transition from shallow to deep convection across scales: The role of congestus clouds. *Journal of the Atmospheric Sciences*, *80*(12), 2989–3005.

Christopoulos, C., & Schneider, T. (2021). Assessing biases and climate implications of the diurnal precipitation cycle in climate models. *Geophysical Research Letters*, *48*(13), e2021GL093017.

Colin, M., Sherwood, S., Geoffroy, O., Bony, S., & Fuchs, D. (2019). Identifying the sources of convective memory in cloud-resolving simulations. *Journal of the Atmospheric Sciences*, *76*(3), 947–962.

Colin, M., & Sherwood, S. C. (2021). Atmospheric convection as an unstable predator–prey process with memory. *Journal of the Atmospheric Sciences*, *78*(11), 3781–3797.

Couvreux, F., Roehrig, R., Rio, C., Lefebvre, M.-P., Komori, T., Derbyshire, S., ... others (2015). Representation of daytime moist convection over the semi-arid tropics by parametrizations used in climate and meteorological models. *Quarterly Journal of the Royal Meteorological Society*, *141*(691), 2220–2236.

Daleu, C. L., Plant, R., Woolnough, S., Stirling, A., & Harvey, N. (2020). Memory properties in cloud-resolving simulations of the diurnal cycle of deep convection. *Journal of Advances in Modeling Earth Systems*, *12*(8), e2019MS001897.

Damiani, R., Vali, G., & Haimov, S. (2006). The structure of thermals in cumulus from airborne dual-Doppler radar observations. *Journal of the Atmospheric Sciences*, *63*(5), 1432–1450.

Davies, L., Plant, R., & Derbyshire, S. (2013). Departures from convective equilibrium with a rapidly varying surface forcing. *Quarterly Journal of the Royal Meteorological Society*, *139*(676), 1731–1746.

Donner, L. J. (1993). A cumulus parameterization including mass fluxes, vertical momentum dynamics, and mesoscale effects. *Journal of the Atmospheric Sciences*, *50*(6), 889–906.

Donner, L. J., & Phillips, V. T. (2003). Boundary layer control on convective available potential energy: Implications for cumulus parameterization. *Journal of Geophysical Research: Atmospheres*, *108*(D22), 4701.

Emanuel, K. A. (1991). A scheme for representing cumulus convection in large-scale models. *Journal of the Atmospheric Sciences*, *48*(21), 2313–2329.

Emanuel, K. A. (1993). A cumulus representation based on the episodic mixing model: the importance of mixing and microphysics in predicting humidity. In *The representation of cumulus convection in numerical models* (pp. 185–192). Springer.

Grabowski, W. (2023). Daytime convective development over land: The role of surface forcing. *Quarterly Journal of the Royal Meteorological Society*, *149*(756), 2800–2819.

Grabowski, W., Bechtold, P., Cheng, A., Forbes, R., et al. (2006). Daytime convective development over land: A model intercomparison based on LBA observations. *Quarterly Journal of the Royal Meteorological Society*, *132*(615), 317–344.

Haerter, J. O. (2021). 1D (time) and 2D (time and vertical coordinate) data for the cases DIU-500m, RCE-500m and DIU2RCE-500m [Data set]. *Zenodo*. doi: https://doi.org/10.5281/zenodo.4898182

Harrington, E. L. (1958). Observations on the appearance and growth of tropical cumuli. *Journal of the Atmospheric Sciences*, *15*(2), 127–130.

Harvey, N. J., Daleu, C. L., Stratton, R. A., Plant, R. S., Woolnough, S. J., & Stirling, A. J. (2022). The impact of surface heterogeneity on the diurnal cycle of deep convection. *Quarterly Journal of the Royal Meteorological Society*, *148*(749), 3509–3527.

Hernandez-Deckers, D., & Sherwood, S. C. (2016). A numerical investigation of cumulus thermals. *Journal of the Atmospheric Sciences*, *73*(10), 4117–4136.

Heus, T., Jonker, H. J. J., Van den Akker, H. E., Griffith, E. J., Koutek, M., & Post, F. H. (2009). A statistical approach to the life cycle analysis of cumulus clouds selected in a virtual reality environment. *Journal of Geophysical Research: Atmospheres*, *114*(D6).

Hohenegger, C., & Bretherton, C. S. (2011). Simulating deep convection with a shallow convection scheme. *Atmospheric Chemistry and Physics*, *11*(20), 10389–10406.

Hohenegger, C., & Stevens, B. (2013). Preconditioning deep convection with cumulus congestus. *Journal of the Atmospheric Sciences*, *70*(2), 448–464.

Holloway, C. E., & Neelin, J. D. (2009). Moisture vertical structure, column water vapor, and tropical deep convection. *Journal of the Atmospheric Sciences*, *66*(6), 1665–1683.

Hwong, Y.-L., Colin, M., Aglas-Leitner, P., Muller, C. J., & Sherwood, S. C. (2023). Assessing memory in convection schemes using idealized tests. *Journal of Advances in Modeling Earth Systems*, *15*(12), e2023MS003726.

Jensen, G. G., Fiévet, R., & Haerter, J. O. (2022). The diurnal path to persistent convective self-aggregation. *Journal of Advances in Modeling Earth Systems*, *14*(5), e2021MS002923.

Jones, T. R., & Randall, D. A. (2011). Quantifying the limits of convective parameterizations. *Journal of Geophysical Research: Atmospheres*, *116*(D8).

Kain, J. S., & Fritsch, J. M. (1993). Convective parameterization for mesoscale models: The Kain-Fritsch scheme. In *The representation of cumulus convection in numerical models* (pp. 165–170). Springer.

Khairoutdinov, M., & Randall, D. (2006). High-resolution simulation of shallow-to-deep convection transition over land. *Journal of the Atmospheric Sciences*,

63(12), 3421–3436.

Kjoenbongarit. (2013). *Forming cumulonimbus (timelapse).* `https://www.youtube.com/watch?v=232LFz-aiz4`. YouTube. (Accessed: 21.07.2023)

Koenig, L. R. (1963). The glaciating behavior of small cumulonimbus clouds. *Journal of Atmospheric Sciences*, *20*(1), 29–47.

Koren, I., & Feingold, G. (2011). Aerosol–cloud–precipitation system as a predator-prey problem. *Proceedings of the National Academy of Sciences of the United States of America*, *108*(30), 12227–12232.

Kurowski, M. J., Suselj, K., Grabowski, W. W., & Teixeira, J. (2018). Shallow-to-deep transition of continental moist convection: Cold pools, surface fluxes, and mesoscale organization. *Journal of the Atmospheric Sciences*, *75*(12), 4071–4090.

Malkus, J. S., & Scorer, R. S. (1955). The erosion of cumulus towers. *Journal of the Atmospheric Sciences*, *12*, 43–57.

Markowski, P., & Richardson, Y. (2011). *Mesoscale meteorology in midlatitudes.* John Wiley & Sons.

Meyer, B., & Haerter, J. O. (2020). Mechanical forcing of convection by cold pools: Collisions and energy scaling. *Journal of Advances in Modeling Earth Systems*, *12*(11), e2020MS002281.

Moorthi, S., & Suarez, M. J. (1992). Relaxed arakawa-schubert. a parameterization of moist convection for general circulation models. *Monthly Weather Review*, *120*(6), 978–1002.

Morrison, H. (2017). An analytic description of the structure and evolution of growing deep cumulus updrafts. *Journal of the Atmospheric Sciences*, *74*(3), 809–834.

Morrison, H., Peters, J. M., Chandrakar, K. K., & Sherwood, S. C. (2022). Influences of environmental relative humidity and horizontal scale of subcloud ascent on deep convective initiation. *Journal of the Atmospheric Sciences*, *79*(2), 337–359.

Morrison, H., Peters, J. M., Varble, A. C., Hannah, W. M., & Giangrande, S. E. (2020). Thermal chains and entrainment in cumulus updrafts. Part I: Theoretical description. *Journal of the Atmospheric Sciences*, *77*(11), 3637–3660.

Moser, D. H., & Lasher-Trapp, S. (2017). The influence of successive thermals on entrainment and dilution in a simulated cumulus congestus. *Journal of the Atmospheric Sciences*, *74*(2), 375–392.

Neggers, R., Stevens, B., & Neelin, J. D. (2006). A simple equilibrium model for shallow-cumulus-topped mixed layers. *Theoretical and Computational Fluid Dynamics*, *20*(5), 305–322.

Nelson, T. C., Marquis, J., Varble, A., & Friedrich, K. (2021). Radiosonde observations of environments supporting deep moist convection initiation during RELAMPAGO-CACTI. *Monthly Weather Review*, *149*(1), 289–309.

Pan, D.-M., & Randall, D. D. (1998). A cumulus parameterization with a prognostic closure. *Quarterly Journal of the Royal Meteorological Society*, *124*(547), 949–981.

Peters, J. M., Hannah, W., & Morrison, H. (2019). The influence of vertical wind shear on moist thermals. *Journal of the Atmospheric Sciences*, *76*(6), 1645–1659.

Peters, J. M., Morrison, H., Nelson, T. C., Marquis, J. N., Mulholland, J. P., & Nowotarski, C. J. (2022). The influence of shear on deep convection initiation. Part I: Theory. *Journal of the Atmospheric Sciences*, *79*(6), 1669–1690.

Pinsky, M., Eytan, E., Koren, I., & Khain, A. (2022). Convective and turbulent motions in nonprecipitating Cu. Part II: LES simulated cloud represented by a starting plume. *Journal of the Atmospheric Sciences*, *79*(3), 793–813.

Plant, R. (2010). A review of the theoretical basis for bulk mass flux convective parameterization. *Atmospheric Chemistry and Physics*, *10*(8), 3529–3544.

Powell, S. W. (2022). Criticality in the shallow-to-deep transition of simulated tropical marine convection. *Journal of the Atmospheric Sciences*, *79*(7), 1805–1819.

Raymond, D. J., & Blyth, A. M. (1989). Precipitation development in a New Mexico thunderstorm. *Quarterly Journal of the Royal Meteorological Society*, *115*(490), 1397–1423.

Rio, C., Del Genio, A. D., & Hourdin, F. (2019). Ongoing breakthroughs in convective parameterization. *Current Climate Change Reports*, *5*, 95–111.

Rio, C., Grandpeix, J.-Y., Hourdin, F., Guichard, F., Couvreux, F., Lafore, J.-P., ... others (2013). Control of deep convection by sub-cloud lifting processes: the ALP closure in the LMDZ5B general circulation model. *Climate dynamics*, *40*, 2271–2292.

Rio, C., Hourdin, F., Grandpeix, J.-Y., & Lafore, J.-P. (2009). Shifting the diurnal cycle of parameterized deep convection over land. *Geophysical Research Letters*, *36*(7).

Rochetin, N., Couvreux, F., Grandpeix, J.-Y., & Rio, C. (2014). Deep convection triggering by boundary layer thermals. Part I: LES analysis and stochastic triggering formulation. *Journal of the Atmospheric Sciences*, *71*(2), 496–514.

Sakradzija, M., Seifert, A., & Heus, T. (2015). Fluctuations in a quasi-stationary shallow cumulus cloud ensemble. *Nonlinear Processes in Geophysics*, *22*(1), 65–85.

Savre, J. (2023a). Outputs from new LBA simulations. Part I: Baseline case [Data set]. *Zenodo*. doi: https://doi.org/10.5281/zenodo.10409139

Savre, J. (2023b). Outputs from new LBA simulations. Part III: Suppressed cold pools [Data set]. *Zenodo*. doi: https://doi.org/10.5281/zenodo.10417550

Savre, J., & Craig, G. (2023). Fitting cumulus cloud size distributions from idealized cloud resolving model simulations. *Journal of Advances in Modeling Earth Systems*, *15*(5), e2022MS003360.

Savre, J., Ekman, A. M. L., & Svensson, G. (2014). Technical note: Introduction to MIMICA, a large-eddy simulation solver for cloudy planetary boundary layers. *Journal of Advances in Modeling Earth Systems*, *6*, 630–649. doi: 10.1002/2013MS000292

Schiro, K. A., & Neelin, J. D. (2019). Deep convective organization, moisture vertical structure, and convective transition using deep-inflow mixing. *Journal of the Atmospheric Sciences*, *76*(4), 965–987.

Schlemmer, L., & Hohenegger, C. (2014). The formation of wider and deeper clouds as a result of cold-pool dynamics. *Journal of the Atmospheric Sciences*, *71*(8), 2842–2858.

Scorer, R., & Ludlam, F. (1953). Bubble theory of penetrative convection. *Quarterly Journal of the Royal Meteorological Society*, *79*(339), 94–103.

Sherwood, S. C., Hernández-Deckers, D., Colin, M., & Robinson, F. (2013). Slippery thermals and the cumulus entrainment paradox. *Journal of the Atmospheric Sciences*, *70*(8), 2426–2442.

Strong, M. (2017). *Time lapse of rising cumulus congestus III – rising turrets with pileus.* `https://www.youtube.com/watch?app=desktop&v=2rHqVFu1m6w`. YouTube. (Accessed: 16.10.2023)

Suselj, K., Kurowski, M. J., & Teixeira, J. (2019). A unified eddy-diffusivity/mass-flux approach for modeling atmospheric convection. *Journal of the Atmospheric Sciences*, *76*(8), 2505–2537.

Takeuchi, Y. (1996). *Global dynamical properties of lotka-volterra systems.* World Scientific.

Tao, C., Xie, S., Ma, H.-Y., Bechtold, P., Cui, Z., Vaillancourt, P. A., ... others (2023). Diurnal cycle of precipitation over the tropics and central United States: intercomparison of general circulation models. *Quarterly Journal of the Royal Meteorological Society*. doi: 10.1002/qj.4629

Tian, Y., Zhang, Y., Klein, S. A., & Schumacher, C. (2021). Interpreting the diurnal cycle of clouds and precipitation in the ARM GoAmazon observations: Shallow to deep convection transition. *Journal of Geophysical Research: Atmospheres*, *126*(5), e2020JD033766.

Torri, G., Kuang, Z., & Tian, Y. (2015). Mechanisms for convection triggering by cold pools. *Geophysical Research Letters*, *42*(6), 1943–1950.

Vogel, R., Albright, A. L., Vial, J., George, G., Stevens, B., & Bony, S. (2022). Strong cloud–circulation coupling explains weak trade cumulus feedback. *Nature*, *612*(7941), 696–700.

Vraciu, C. V., Kruse, I. L., & Haerter, J. O. (2023). The role of passive cloud volumes in the transition from shallow to deep atmospheric convection. *Geophysical Research Letters*, *50*(23), e2023GL105996.

Wagner, T. M., & Graf, H.-F. (2010). An ensemble cumulus convection parameterization with explicit cloud treatment. *Journal of the Atmospheric Sciences*, *67*(12), 3854–3869.

Waite, M. L., & Khouider, B. (2010). The deepening of tropical convection by congestus preconditioning. *Journal of the Atmospheric Sciences*, *67*(8), 2601–2615.

Yano, J.-I. (2014). Formulation structure of the mass-flux convection parameterization. *Dynamics of Atmospheres and Oceans*, *67*, 1–28.

Yano, J.-I., Bister, M., Fuchs, Ž., Gerard, L., Phillips, V., Barkidija, S., & Piriou, J.-M. (2013). Phenomenology of convection-parameterization closure. *Atmospheric Chemistry and Physics*, *13*(8), 4111–4131.

Yano, J.-I., & Plant, R. (2012a). Finite departure from convective quasi-equilibrium: Periodic cycle and discharge–recharge mechanism. *Quarterly Journal of the Royal Meteorological Society*, *138*(664), 626–637.

Yano, J.-I., & Plant, R. S. (2012b). Interactions between shallow and deep convection under a finite departure from convective quasi equilibrium. *Journal of the Atmospheric Sciences*, *69*(12), 3463–3470.

Zhao, M., & Austin, P. H. (2005). Life cycle of numerically simulated shallow cumulus clouds. Part II: Mixing dynamics. *Journal of the Atmospheric Sciences*, *62*(5), 1291–1310.

Zhuang, Y., Fu, R., Marengo, J. A., & Wang, H. (2017). Seasonal variation of shallow-to-deep convection transition and its link to the environmental conditions over the Central Amazon. *Journal of Geophysical Research: Atmospheres*, *122*(5), 2649–2666.